SAND2019-14959J

ORIGINAL REPORT

Void Growth by Dislocation Adsorption

R. B. Sills[a*] and B. L. Boyce[b]

[a]Sandia National Laboratories, Livermore, CA 94551; [b]Sandia National Laboratories, Albuquerque, NM 87165

ARTICLE HISTORY
Compiled December 9, 2019

ABSTRACT
We propose a dislocation adsorption-based mechanism for void growth in metals, wherein a void grows as dislocations from the bulk annihilate at its surface. The basic process is governed by glide and cross-slip of dislocations at the surface of a void. Using molecular dynamics simulations we show that when dislocations are present around a void, growth occurs more quickly and at much lower stresses than when the crystal is initially dislocation-free. Finally, we show that adsorption-mediated growth predicts an exponential dependence on the hydrostatic stress, consistent with the well-known Rice-Tracey equation.

KEYWORDS
void; dislocation; plasticity; rupture

Impact Statement

Void growth during ductile rupture is mediated by dislocation adsorption, not dislocation emission as previously theorized. The mechanism is consistent with Rice-Tracey scaling and observations of voids near cell walls.

1. Introduction

The ductile fracture process in metals is relevant to a number of failure scenarios including quasi-static tearing [1,2], dynamic spall [3], creep rupture [4], irradiation creep [5], and wear debris generation [6]. Typically, the fracture surfaces of these metals exhibit a characteristic pitted "ductile dimple" appearance indicative of the microvoid coalescence rupture process [7]. Often ductile fracture is due to the nucleation, growth, and coalescence of microscale voids [7]. It is usually assumed that the material contains a pre-existing population of hard particles or inclusions made from secondary phases. Void nucleation then occurs when these particles crack or the interface between the particles and matrix delaminates [8–10]. The voids grow under the action of plastic deformation around the voids, driven by hydrostatic stresses [11,12]. Final rupture oc-

CONTACT R. B. Sills Email: ryan.sills@rutgers.edu
*PRESENT ADDRESS Department of Materials Science and Engineering, Rutgers University, Piscataway, NJ 08854

curs when the voids coalesce, which typically occurs when ligaments between adjacent voids reach some critical thickness leading to shear banding or ligament fracture.

This basic picture for rupture in ductile solids has been around for nearly 50 years. Despite this fact, many of the details surrounding it are poorly understood, including the micromechanics of void nucleation and growth. For example, ductile rupture is still observed in materials that do not contain hard particles or pre-existing voids, making it unclear how the voids nucleate in the first place [13,14]. There are numerous competing continuum-scale phenomenological models for the ductile rupture process [15] including the Gurson model [16], an adaptation by Tvergaard and Needleman [17], modifications to account for shear localization [18], and stress triaxiality models [19]. The Sandia Fracture Challenge has illustrated the ongoing disagreement with regard to the most appropriate failure models and their difficulties in blindly predicting rupture scenarios [20,21]. Many of these difficulties arise from assumptions made about the underlying micromechanical mechanisms that drive void nucleation and growth; for example, many models assume a pre-existing void density and hence neglect void nucleation altogether. At lower length scales such as the scale of individual grains, there is even broader disagreement as to the proper models to describe the rupture process. These discrepancies are due in part to a lack of clear fundamental understanding of the detailed unit mechanisms governing nucleation, growth, and coalescence.

In this work, we focus on obtaining a detailed micromechanical understanding of the void growth process. Much of the literature on void growth focuses on continuum theories which characterize the void growth rate as a function of the stress state [12,22]. Of these, perhaps the most famous is the work by Rice and Tracey [11], later corrected by Huang [23], who solved for the growth rate of an isolated void in a rigid-perfectly plastic solid loaded with applied strain rate tensor $\dot{\epsilon}_{ij}$ and hydrostatic stress σ^H. They obtained the simple result for the void growth rate that

$$\frac{\dot{R}}{R} = \alpha \exp\left(\frac{3\sigma^H}{2\sigma_Y}\right)\dot{\epsilon}^{eq} \tag{1}$$

where R is the void radius, σ_Y is the yield strength, $\dot{\epsilon}^{eq} = \sqrt{\frac{2}{3}\dot{\epsilon}_{ij}\dot{\epsilon}_{ij}}$ is the equivalent plastic strain rate (using Einstein notation), and $\alpha = 0.427$ is a numerically obtained constant [23]. Hence, the continuum theory predicts an exponential dependence on the hydrostatic stress. The Rice-Tracey equation was recently validated against detailed X-ray tomographic measurements of void growth [24]. According to Rice-Tracey, voids grow as plastic strain accumulates around them, but the detailed micromechanics are unclear.

In an effort to fill this micromechanical knowledge gap, numerous atomistic studies of void growth have been performed in the last decade [26–31]. The key finding in all of these studies is that voids grow by *nucleating* dislocations at the surface of the void. However, such a mechanism poses a fundamental dilemma. In particular, Nguyen and Warner [32] showed using molecular dynamics and transition state theory calculations, that dislocation nucleation from the surface of a void in pure aluminum is a tremendously slow process. For example, the nucleation rate under 0.78 GPa of shear stress is one dislocation per year! In order to obtain nucleation rates on the order of 1 s^{-1}, applied stresses need to exceed 1 GPa. While stresses of this magnitude may be relevant to high loading rates (e.g., shock loading [33]), they are well beyond the strengths of many structural metals under quasi-static loading.

In this work, we resolve this problem by proposing that void growth via adsorp-

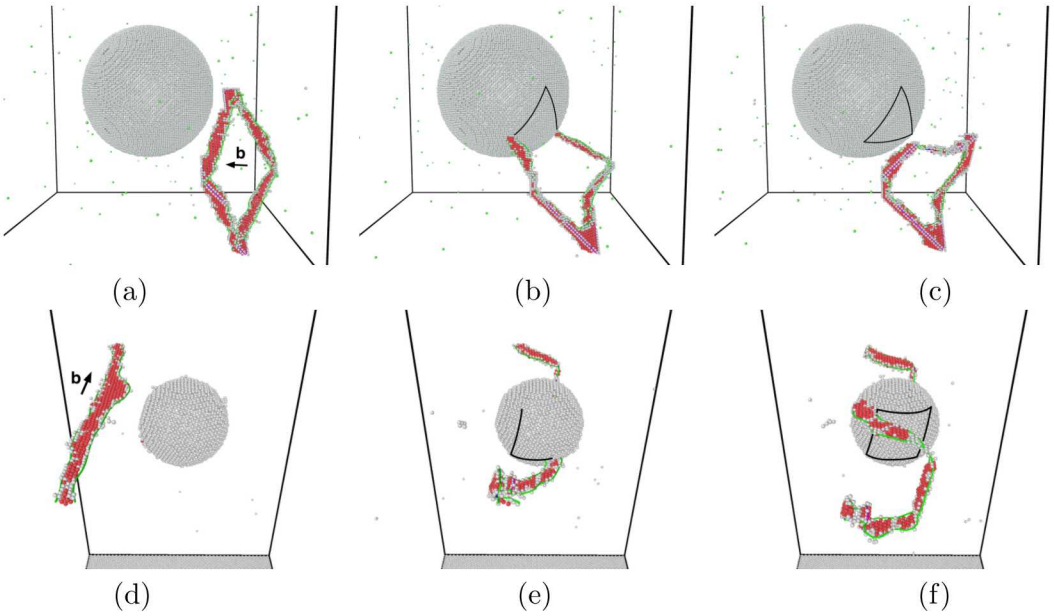

Figure 1. Dislocation-void interactions under an applied hydrostatic stress. Black lines denote approximate dislocation trajectories on the surface of the void. (a-c) Prismatic dislocation loop loaded at $\sigma^H = 2$ GPa with void of radius $R_0 = 7.5$ nm. (a) Initial configuration. (b) Configuration after loop glides into the void. (c) After the loop cross-slips and forms a closed-path on the void's surface. (d-f) Screw dislocation loaded at $\sigma^H = 3.7$ GPa with void of radius $R_0 = 3$ nm. (d) Initial configuration. (e) Configuration after the dislocation cross-slips and glides across the face twice. (f) After the dislocation cross-slips and glides two more times tracing out a prismatic dislocation loop. Atoms at the void surface and in dislocation cores are colored white, and inside stacking fault ribbons are colored red. Shockley partial dislocation lines are shown in green. Image made using OVITO [25].

tion of dislocations from the surrounding bulk is the primary mechanism of growth. Adsorption-mediated growth was recently shown to be a viable mechanism for small amounts of void growth ($< 0.1\%$ by radius) by Chang et al. [34]. While Chang et al.'s prior work opens the possibility that dislocation adsportion may be an important growth mechanism, their use of discrete dislocation dynamics was limited to low dislocation densities below those experimentally observed at relevant cell wall boundaries [14,35], and suggested that the adsorption mechanism may be limited to only the very early stages of void growth. Many important questions remain to be answered before the importance of adsorption-mediated growth can be understood, however. Namely: what are the key dislocation processes underlying the mechanism?; what is the connection, if any, between nucleation-mediated and adsorption-mediated growth?; and, what growth rates are predicted by adsorption-mediated growth and how do they compare with experiments? In this work, we address these questions, demonstrating that 1) the dislocation processes enabling adsorption-mediated growth (glide and cross-slip) occur rapidly, 2) even in a scenario where nucleation-mediated growth occurs (no dislocations present initially), adsorption-mediated growth quickly takes over as the mechanism of growth, and 3) growth rates predicted by adsorption-mediated growth are consistent with the experimentally validated Rice-Tracey equation. Lastly, we argue that our results elucidate recent experimental observations of void growth at regions with elevated dislocation density (cell block boundaries) [14]. Combined together, we believe our results demonstrate that adsorption-mediated growth is an important growth mechanism.

2. Methods and Results

We study void growth at a temperature of 300 K in face-centered cubic aluminum using the embedded atom method potential of Mishin et al. [36] and the molecular dynamics code LAMMPS [37,38] (see Supplementary online material for simulation details).

To begin our studies, we focus on the interaction of isolated dislocations with a single void in order to elucidate underlying mechanisms. We introduce a void of radius R_0 and impose a constant hydrostatic tensile stress on the simulation cell. Treating the void as a spherical cavity in an isotropically elastic matrix under a pure hydrostatic load, we can compute the equivalent Eshelby eigenstrain [39,40] to obtain a stress field around the void of (see Supplementary online material)

$$\sigma_{ij} = \frac{1}{2}\sigma^H \left(\frac{R}{r}\right)^3 \left(\delta_{ij} - \frac{3x_i x_j}{r^2}\right) \tag{2}$$

where δ_{ij} is the Kronecker delta and $r = \sqrt{x_i x_i}$. The resulting maximum shear stress at the surface of the void is $\frac{3}{4}\sigma^H$. We study two dislocation geometries: a prismatic (meaning the initial plane of the loop is orthogonal to the Burgers vector) dislocation loop and a straight screw dislocation. Note that if a void were not present, there would be no driving forces acting on the dislocation lines since the system is under a pure hydrostatic stress state. Fig. 1 depicts the response of the dislocation lines. In both cases, the dislocation lines are attracted to the void. After initially colliding with the void, the dislocations quickly glide across its face, and then cross-slip onto another glide plane where they are able to glide again. After this process repeats several times, the end result is that closed dislocation loops are traced out on the void's surface. The

volume change of the void after the dislocation loops are traced out is [41,42]

$$\delta V = \int_S \mathbf{b} \cdot d\mathbf{A} = \int_S (\mathbf{b} \cdot \mathbf{n})\, dA \tag{3}$$

where $\mathbf{b}$ is the Burgers vector, $\mathbf{n}$ is the outward normal of the void surface, and S is the area traced out by the dislocation line. Note that the exact same volume change would occur if instead a loop with an oppositely signed Burgers vector and the same shape were nucleated from the surface of the void [43]. Hence the underlying mechanics is exactly the same between adsorption-mediated and nucleation-mediated growth. The key point is that adsorption-mediated growth can occur much more rapidly since it relies on cross-slip and glide, which are known to occur readily over typical experimental timescales. Furthermore, the externally-sourced dislocations can be produced much more quickly (via conventional multiplication processes) than surface-based nucleation. Since we are constrained to atomistic timescales in these simulations, the stresses need to be large (≥ 2 GPa), however, to accelerate the processes. Demonstration of the basic unit-mechanisms underlying adsorption-mediated growth is the first major contribution in this work.

Next, we demonstrate the behavior of a crystal containing voids under an applied hydrostatic tensile strain rate, a case that has been considered by several researchers [28,30,31]. We focus on two cases: a) no dislocations initially present and b) n prismatic dislocation loops with edges of length 20 nm and 21.2 nm (same shape as shown in Fig. 1(a)) initially present. A comparison between these two cases has not been made before. For reference, when $n = 18$ the initial dislocation density is about 4.3×10^{16} m^{-2}. This high initial dislocation density may be representative of a dislocation cell wall given the experimental observations of densities in excess of 10^{15} m^{-2} locally in highly deformed aluminum [35,44]. Fig. 2 presents resulting stress-strain curves under a strain rate of 3×10^8 s^{-1} with voids of initial radii $R_0 = 2.5$ and 10 nm, and a simulation box that is $L = 32.5$ nm on each edge. Fig. 2(a) reproduces the same behavior as previous studies when dislocations are not initially present, with a large spike at yield, followed by a rapid drop in stress and subsequent softening. This initial spike corresponds to the nucleation of one or more dislocations from the surface of the void, which then enables plastic growth of the void. The new result shown here is the influence of pre-seeding the system with dislocations. We show that as the number of initial dislocation loops increases, the stress spike at yield is greatly reduced. This indicates that void growth occurs much more readily when dislocations are present, since void growth initiates at much lower stresses. Beyond initial yield, however, the stress-strain curves are independent of the number of dislocation loops.

The observation that the post-yield behavior is insensitive to the initial dislocation content motivated additional simulations, where we increased the void radius while concurrently increasing the box dimensions so that the number of atoms was kept approximately constant at 1.9 million. In this way, all of the initial conditions can be related to each other and the influence of dislocations—nucleated or initially introduced—can be evaluated. For instance, at 10.5% strain the simulation with an initial void radius 5 nm has grown to an effective void radius of $R_{\text{eff}} = \left(\frac{3}{4\pi}\Delta V + R_0^3\right)^{1/3} = 10$ nm, where ΔV is the volume change of the cell. Hence, the simulation with initial void radius of 10 nm emulates the $R_0 = 5$ nm void case at 10.5% strain. We can then directly determine the influence that dislocations have at that strain by starting the simulation with and without dislocation loops introduced. Fig. 2(b) presents the resulting stress-strain curves with and without dislocation loops,

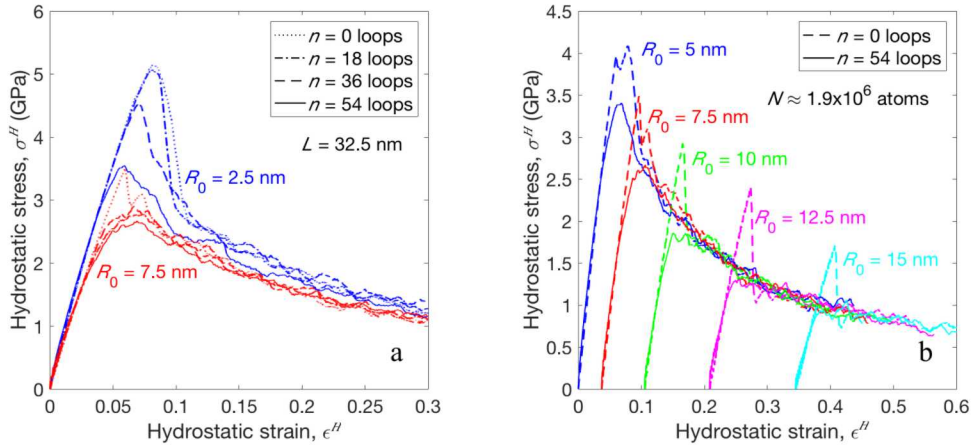

Figure 2. Hydrostatic stress-strain curves under a constant hydrostatic strain rate of 3×10^8 s^{-1}. (a) Fixed box size of $L = 32.5$ nm, two different initial void radii, and different numbers of dislocation loops. (b) Box dimension varied to keep number of atoms approximately constant at 1.9 million with different initial void radii. Curves are shifted so that the void radius is approximately the same at the same strain.

all translated along the x-axis so that the instantaneous void sizes match. Interestingly, beyond initial yield where a stress spike is observed in dislocation-free systems, all simulations collapse onto a single universal stress-strain curve. This fact indicates that post-yield, where the bulk of the void growth occurs, voids in simulations with *and* without dislocation loops grow by the same mechanism: dislocation adsorption. Specifically, under the influence of the void's stress field, dislocations multiply and adsorb at its surface. These results indicate that void growth does not occur by dislocation nucleation alone; void growth may be initiated by nucleation, but the growth itself occurs when the nucleated dislocations multiply and interact with the void's stress field. The finding that adsorption-mediated growth dominates even in dislocation-free systems is the second major contribution of this work.

These results provide details about the adsorption-mediated growth process, but do not provide a means for computing void growth rates akin to Eq. (1). To this end, we have computed void growth rates under a fixed tensile hydrostatic stress. By examining the volume history of the system we can estimate the void growth rate. Fig. 3(a) shows the volume history expressed in terms of the effective void radius with a void of initial radius 5 nm under a stress of 2.8 GPa. Curves are shown for $n = 0$, 18, 36 and 54 dislocation loops. When no dislocation loops are present, no void growth is observed because the stress is insufficient to drive nucleation. As the number of loops increases, the void growth rate increases. We can approximate the effective void growth rate $\dot{R}_{\text{eff}}$ using linear fits to these time histories. Fig. 3(b) summarizes the results from 360 MD simulations; 20 random loop configurations for each value of n with hydrostatic stresses ranging from 2.3 to 2.8 GPa. Since void growth is highly sensitive to the specific dislocation configuration around the void, growth rates vary significantly for the same stress and number of loops (see Supplementary online material). Hence, in Fig. 3(b) we plot the median growth rate among the 20 replicates at each set of conditions. To demonstrate that our results are not biased by the use of prismatic dislocation loops, we have also performed simulations using 12 shear loops, giving an initial dislocation density of 5.2×10^{16} m^{-2} (see Supplementary online material). These results are also presented in Fig. 3(b), showing more scatter but the same overall trend. Fig. 3(b)

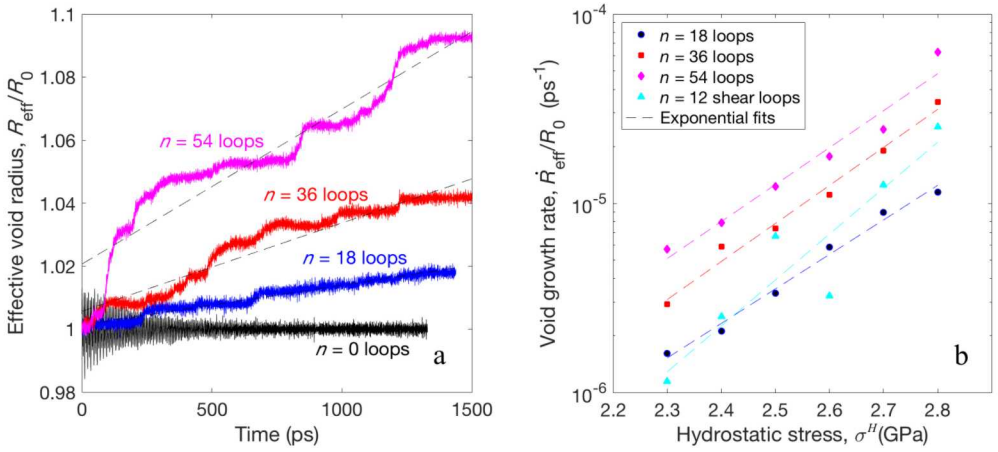

Figure 3. Void growth rates under a constant hydrostatic stress σ^H when $R_0 = 5$ nm and $L = 32.5$ nm. (a) Effective void radius as a function of time with $\sigma^H = 2.8$ GPa. (b) Void growth rate as a function of hydrostatic stress. Dashed lines are exponential fits (Eq. (4)).

demonstrates that the void growth rate increases with dislocation density and that the adsorption-mediated void growth rate is exponentially dependent on the hydrostatic stress. The latter result is significant because it is consistent with the experimentally validated Rice-Tracey relation, Eq. (1). The fact that adsorption-mediated growth follows the same stress dependence as is observed in quasi-static experiments is the third major contribution of this work. Note that the same statement cannot be made about nucleation-mediated growth. Analyzing the exponential curve fits further, we find that the growth rates with prismatic loops at all dislocation densities exhibit an exponent of about $4.4\sigma^H$, which according to Eq. (1) implies a "yield strength" of about 341 MPa; this is not an unreasonable order of magnitude for local stresses in highly work hardened aluminum which has been shown to exhibit a macroscopic ultimate strength as high as 250 MPa [45]. Hence, our results predict a growth rate of the form

$$\frac{\dot{R}}{R} = A(\rho) \exp\left(4.4\sigma^H\right) \tag{4}$$

where $A(\rho)$ is a dislocation-density-dependent prefactor.

3. Discussion

The current work suggests that the dislocation-adsportion mechanism proposed by Chang et al. [34] can continue to operate at much higher dislocation densities, relevant to dislocation cell walls where voids are now understood to proliferate. Moreover, the current results suggest that the adsorption mechanism can account for extensive void growth, well beyond 0.1% indicated in the previous studies [34]. These current results, and the observed consistency with Rice-Tracey scaling, suggest that the adsorption mechanism is a more comprehensive explanation for void growth than previously indicated, strengthening the argument that dislocation emission is not a controlling factor. We note that in Rice and Tracey's analysis [11], a hydrostatic stress and far-field strain rate were simultaneously imposed, making Eq. (1) depend on both σ^H and $\dot{\epsilon}^{eq}$. How-

ever, in MD it is not possible to impose a strain rate and a stress state concurrently, which is why we have only focused on the influence of σ^H.

Overall, we believe the dislocation adsorption mechanism acts to enhance the kinetics of void growth; the driving force for growth is still hydrostatic stress with adsorption of pre-existing dislocations accelerating the growth rate and eliminating the need for nucleation or diffusive processes. The fundamental dislocation processes involved in adsorption-mediated growth—glide and cross-slip of dislocations—occur readily in typical experimental conditions. Cross-slip is the slower of the two processes, however it has been shown that the energy barrier for cross-slip at free surfaces is extremely low (< 0.1 eV), making the cross-slip rate high [46].

The incipient nanoscale voids considered here are distinct from the micrometer scale voids typically investigated experimentally, e.g., [47]. The present results suggest that incipient nanoscale voids can grow under high local stresses, but only if in the presence of extremely high dislocation densities, such as those found in a dislocation cell wall; this assertion is supported by recent experimental evidence showing that voids prefer to reside in regions of high dislocation density [14,48]. Additional research is needed to confirm that such behavior occurs not only at the timescales of MD, but also under quasi-static loading conditions and under lower stress conditions at slower timescales. Because the dislocations enable growth without the need for nucleation or diffusive processes, we expect that strain-rate will play only a minor role in this phenomenon. Combined together, the evidence presented here suggests an intimate, mechanistic linkage between void growth and strain-induced dislocation networks which may be influential to theories of ductile fracture.

Acknowledgement

We thank Prof. Wei Cai and Dr. Philip Noell for insightful discussions, and Dr. Claire Chisholm and Dr. Douglas Medlin for feedback on the manuscript.

Disclosure statement

No potential conflict of interest was reported by the authors.

Funding

BLB was supported by the Center for Integrated Nanotechnologies, an Office of Science User Facility operated for the U.S. Department of Energy (DOE) Office of Science. Sandia National Laboratories is a multimission laboratory managed and operated by National Technology and Engineering Solutions of Sandia, LLC, a wholly owned subsidiary of Honeywell International Inc., for the U.S. Department of Energy's National Nuclear Security Administration under contract DE-NA0003525. This paper describes objective technical results and analysis. Any subjective views or opinions that might be expressed in the paper do not necessarily represent the views of the U.S. Department of Energy or the United States Government.

References

[1] Puttick KE. Ductile fracture in metals. Phil Mag. 1959;4(44):964–969.
[2] Bauer RW, Lyles RL, Wilsdorf HGF. Direct observation of crack formation using a high-voltage electron microscope. Z Metallkunde. 1972;.
[3] Grady DE. The spall strength of condensed matter. J Mech Phys Sol. 1988;36:353–384.
[4] Kassner ME, Hayes TA. Creep cavitation in metals. Int J Plast. 2003;19:1715–1748.
[5] Harkness SD, Tesk JA, Li CY. An analysis of fast neutron effects on void formation and creep in metals. Nuclear Applications and Technology. 1970;9:24–30.
[6] Suh NP. An overview of the delamination theory of wear. Wear. 1977;44:1–16.
[7] Pineau A, Benzerga AA, Pardoen T. Failure of metals I: Brittle and ductile fracture. Acta Mater. 2016;107:424–483.
[8] Goods SH, Brown LM. The Nucleation of Cavities by Plastic Deformation. Acta Metall. 1979;27:1–15.
[9] Garrison Jr WM, Moody NR. Ductile Fracture. J Phys Chem Solids. 1987;48:1035–1074.
[10] Thomason PF. Ductile fracture of metals. Elmsford, NY: Pergamon Press; 1990.
[11] Rice JR, Tracey DM. On the ductile enlargement of voids in triaxial stress fields. J Mech Phys Sol. 1969;17:201–217.
[12] Needleman A, Tvergaard V, Hutchinson JW. Void growth in plastic solids. In: Argon AS, editor. Topics in fracture and fatigue. Chapter 4. New York: Springer-Verlag; 1992. p. 145–1778.
[13] Wilsdorf HGF. The ductile fracture of metals: A microstructural viewpoint. Mat Sci Eng. 1983;59:1–39.
[14] Noell P, Carroll J, Hattar K, et al. Do voids nucleate at grain boundaries during ductile rupture? Acta Mater. 2017;137:103–114.
[15] Wierzbicki T, Bao Y, Lee YW, et al. Calibration and evaluation of seven fracture models. Int J Mech Sci. 2005;47:719–743.
[16] Gurson AL. Continuum theory of ductile rupture by void nucleation and growth: Part I—Yield criteria and flow rules for porous ductile media. J Eng Mater Technol. 1977; 99:2–15.
[17] Tvergaard V, Needleman A. Analysis of the cup-cone fracture in a round tensile bar. Acta Metall. 1984;32:157–169.
[18] Nashon K, Hutchinson JW. Modification of the Gurson model for shear failure. Europ J Mech. 2008;27:1–17.
[19] Bao Y, Wierbicki T. On fracture locus in the equivalent strain and stress triaxiality space. Int J Mech Sci. 2004;46:81–98.
[20] Boyce BL, Kramer SLB, Fang HE, et al. The sandia fracture challenge: blind round robin predictions of ductile tearing. Int J Fract. 2014;186(1):5–68.
[21] Boyce BL, Kramer SLB, Bosiljevac TR, et al. The second sandia fracture challenge: predictions of ductile failure under quasi-static and moderate-rate dynamic loading. Int J Fract. 2016;198(1):5–100.
[22] Besson J. Contuum Models of Ductile Fracture: A Review. Int J Damage Mech. 2010; 19:3–52.
[23] Huang Y. Accurate dilation rates for spherical voids in triaxial stress fields. Department of Applied Sciences, Harvard University; 1989. Mech-155.
[24] Weck A, Wilkinson DS, Maire E, et al. Visualization by X-ray tomography of void growth and coalescence leading to fracture in model materials. Acta Mater. 2008;56:2919–2928.
[25] Stukowski A. Visulatization and analysis of atomistic simulation data with Ovito: The Open Visulation Tool. Modelling Simul Mater Sci Eng. 2010;18:015012.
[26] Marian J, Knap J, Ortiz M. Nanovoid Cavitation by Dislocation Emission in Aluminum. Phys Rev Lett. 2004;93.
[27] Lubarda V, Schneider M, Kalantar D, et al. Void growth by dislocation emission. Acta Mater. 2004;52:1397–408.
[28] Traiviratana S, Bringa EM, Benson DJ, et al. Void growth in metals: Atomistic calcula-

tions. Acta Mater. 2008;56:3874–3886.
[29] Meyers MA, Traiviratana S, Lubarda VA, et al. The role of dislocations in the growth of nanosized voids in ductile failure of metals. JOM. 2009;61.
[30] Bringa EM, Traiviratan S, Meyers MA. Void initiation in fcc metals: Effect of loading orientation and nanocrystalline effects. Acta Mater. 2010;58:4458–4477.
[31] Mi C, Buttry DA, Sharma P, et al. Atomistic insights into dislocation-based mechanisms of void growth and coalescence. J Mech Phys Sol. 2011;69:1858–1871.
[32] Nguyen LD, Warner DH. Improbability of Void Growth in Aluminum via Dislocation Nucleation under Typical Laboratory Conditions. Phys Rev Lett. 2012;108.
[33] Reina C, Marian J, Ortiz M. Nanovoid nucleation by vacancy aggregation and vacancy-cluster coarsening in high-purity metallic single crystals. Phys Rev B. 2011;84.
[34] Chang HJ, Segurado J, Llorca J. Three-dimensional dislocation dynamics analysis of size effects on void growth. Scripta Mater. 2015;95:11–14.
[35] Essmann U, Mughrabi H. Annihilation of dislocations during tensile and cyclic deformation and limits of dislocation densities. Phil Mag A. 1979;40(6):731–756.
[36] Mishin Y, Farkas D, Mehl MJ, et al. Interatomic potentials for monoatomic metals from experimental data and ab initio calculations. Phys Rev B. 1999;59.
[37] Plimpton S. Fast parallel algorithms for short-range molecular dynamics. J Comp Phys. 1995;117:1–19.
[38] LAMMPS, `http:/lammps.sandia.gov` ; 2018.
[39] Eshelby JD. Elastic inclusions and inhomogeneities. In: Sneddon IN, Hill R, editors. Progress in solid mechanics. Chapter 3. Amsterdam: North-Holland Publishing Company; 1961. p. 87–140.
[40] Mura T. Micromechanics of defects in solids. Norwell, MA: Kluwer Academic Publishers; 1987.
[41] Anderson PM, Hirth JP, Lothe J. Theory of dislocations, 3rd ed. Cambridge University Press; 2017.
[42] Bulatov VV, Wolfer WG, Kumar M. Shear impossibility: Comments on "Void growth by dislocation emission" and "Void growth in metals: Atomistic calculations". Scripta Mater. 2010;63:144–147.
[43] Ashby MF, Johnson L. On the generation of dislocations at misfitting particles in a ductile matrix. Phil Mag. 1969;20:1009–1022.
[44] Merriman CC, Field DP, Trivedi P. Orientation dependence of dislocation structure evolution during cold rolling of aluminum. Mater Sci Eng A. 2008;494:28–35.
[45] Jiang J, Ding Y, Zuo F, et al. Mechanical properties and microstructures of ultrafine-grained pure aluminum by asymmetric rolling. Scripta Mater. 2009;60:905–908.
[46] Rao SI, Dimiduk DM, Parthasarathy TA, et al. Atomistic simulations of surface cross-slip nucleation in face-centered cubic nickel and copper. Acta Mater. 2013;61:2500–2508.
[47] Stone RHV, Cox TB, Low JR, et al. Microstructural aspects of fracture by dimpled rupture. International Metals Reviews. 1985;30(1):157–180. Available from: https://doi.org/10.1179/imtr.1985.30.1.157.
[48] Noell PJ, Sabisch JEC, Medlin DL, et al. Nanoscale conditions for ductile void nucleation in copper: vacancy condensation and the growth-limited microstructural state. Submitted. 2019;.

Supplemental online material for

Void Growth by Dislocation Adsorption

R. B. Sills[a] and B. L. Boyce[b]

[a]Sandia National Laboratories, Livermore, CA 94551; [b]Sandia National Laboratories, Albuquerque, NM 87165

ARTICLE HISTORY
Compiled June 18, 2019

Molecular dynamics simulations

All molecular dynamics (MD) simulations were conducted in LAMMPS [1] using either a Nosé-Hoover thermostat (strain-controlled simulations) or thermostat/barostat (stress-controlled simulations), with damping parameters of 0.01 ps and 1 ps for the thermostat and barostat, respectively. For stress-controlled simulations, after relaxing the system it is quickly loaded up to the target hydrostatic stress over 1 ps. The time step size was fixed at 1 fs. Periodic boundary conditions were used in all directions for all simulations except for those examining the interaction of a single screw dislocation with a void (Fig. 1(d-f) in the manuscript). In this case, $(1\,\bar{1}\,1)$ free surfaces were introduced, and then the screw dislocation was inserted by imposing the displacement field of a Volterra dislocation [2]. For this simulation, the box was rectangular with axes along the $[1\,1\,0]$, $[1\,\bar{1}\,1]$, and $[1\,\bar{1}\,\bar{2}]$ directions with respective dimensions of 234, 573, and 252 nm. All other simulations used a cubic box with edges of length 32.5 nm along $\langle 0\,0\,1\rangle$ directions. To introduce prismatic dislocation loops, parallelepipedal regions of atoms were removed, with two edges of the parallelepiped along $[1\,1\,1]$ directions with lengths of 20 nm and 21.2 nm, and the third edge along an $[0\,1\,1]$ direction with length $a/\sqrt{2}$ where a is the lattice constant. After relaxing for 10 ps, these regions collapsed together to produce dislocation loops with four glissile edges occupying two different slip systems. For simulations when n loops are introduced, we insert an equal number of loops for each of the six unique $\langle 1\,1\,0\rangle$ Burgers vectors. An example of an initial configuration is shown in Fig. 1. To introduce shear dislocation loops, we use Barnett's displacement field solution for a triangular dislocation loop [3,4] to insert equilateral triangular shear dislocation loops whose edges have a length of 50 nm. Each loop is oriented so that one edge is parallel to the Burgers vector, with one loop inserted for each of the 12 slip systems.

To aid in the interpretation of the screw dislocation simulation discussed in the manuscript, we provide images showing additional orientations of the simulation snapshots. Fig. 2 shows the same snapshots as Fig. 1(d-f) in the manuscript, but viewed (a-c) from above and (d-f) from the left side.

CONTACT R. B. Sills. Email: rbsills@sandia.gov

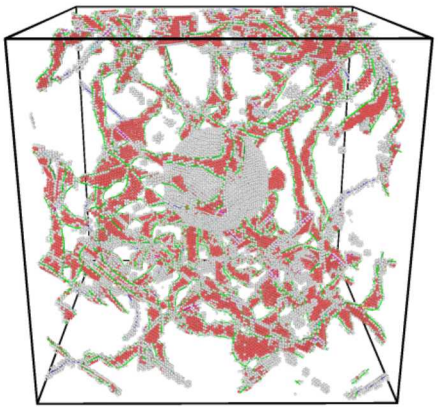

Figure 1. Example of an initial configuration used for void growth simulations with $R_0 = 5$ nm and $n = 18$ dislocation loops. Atoms inside stacking fault ribbons are colored red. Atoms at the void surface and in dislocation cores are colored white. Shockley partial dislocation lines are shown in green. Image made using OVITO [5].

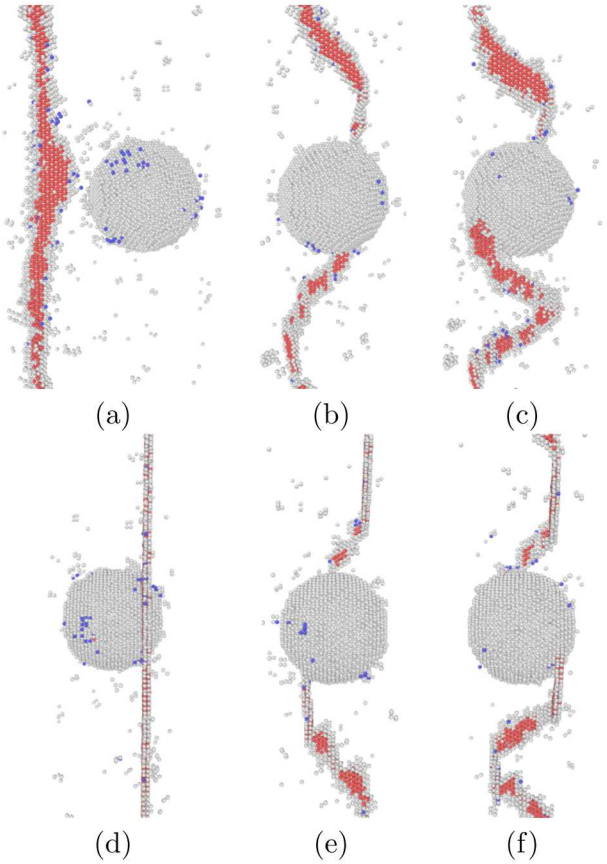

Figure 2. Additional orientations for the simulation snapshots provided in Fig. 1(d-f) of the manuscript showing a screw dislocation interacting with a void. (a-c) View from above and (d-f) side view from the left. Images made using OVITO [5].

Stress field of a void under a hydrostatic stress

Here we prove Eq. (2) of the manuscript using Eshelby's equivalent eigenstrain approach. According to this technique, we consider a spherical inhomogeneity with elastic constants C'_{ijkl} embedded in a matrix with elastic constants C_{ijkl}. We consider isotropically elastic solids, so

$$C_{ijkl} = \lambda\delta_{ij}\delta_{kl} + \mu\left(\delta_{ik}\delta_{jl} + \delta_{il}\delta_{jk}\right) \tag{1}$$

where $\lambda = 2\mu\nu/(1-2\nu)$ is Lamé's constant, μ is the shear modulus, ν is Poisson's ratio, δ_{ij} is the Kronecker delta, and summation over repeated indices is implied. The inhomogeneity does not have a misfit, so that when no stress is applied to the system, the stress state is zero everywhere. However, when uniform strain state e^A_{ij} is applied to the system, the differing elastic constants induce a non-uniform stress state in the matrix around the inhomogeneity. We can solve for this stress state by determining the eigenstrain e^*_{ij} that, when imposed on an inclusion of the same shape as the inhomogeneity but with elastic constants C_{ijkl}, reproduces the same stress state as the inhomogeneous system under applied strain. The eigenstrain e^*_{ij} is called the equivalent eigenstrain.

The equivalent eigenstrain is determined by solving the following expression [6,7]

$$\left[\left(C'_{ijkl} - C_{ijkl}\right)S_{klmn} + C_{ijmn}\right]e^*_{mn} = \left(C_{ijkl} - C'_{ijkl}\right)e^A_{kl}, \tag{2}$$

where S_{ijkl} is the Eshelby tensor and is dependent on the shape of the inhomogeneity. For a sphere we have [7]

$$S_{ijkl} = \frac{5\nu - 1}{15(1-\nu)}\delta_{ij}\delta_{kl} + \frac{4 - 5\nu}{15(1-\nu)}\left(\delta_{ik}\delta_{jl} + \delta_{il}\delta_{jk}\right). \tag{3}$$

For a void inhomogeneity, we have that $C'_{ijkl} = 0$ so the right-hand-side of Eq. (2) becomes $\sigma^A_{ij} = C_{ijkl}e^A_{kl}$, the applied stress tensor if the solid were homogeneous. We consider an applied hydrostatic stress state, $\sigma^A_{ij} = \sigma^H\delta_{ij}$. Solving for the equivalent eigenstrain, we find that $e^*_{ij} = \bar{e}^*\delta_{ij}$ where

$$\bar{e}^* = \frac{3(1-\nu)}{4(1+\nu)}\left(\frac{\sigma^H}{\mu}\right). \tag{4}$$

This means that a void under applied hydrostatic stress behaves like an Eshelby inclusion with a dilatational misfit that is proportional to σ^H/μ. The stress state of a spherical inclusion of radius R with dilatational misfit is [8]

$$\sigma_{ij} = \frac{2\mu(1+\nu)}{3(1-\nu)}\bar{e}^*\left(\delta_{ij} - \frac{3x_ix_j}{r^2}\right)\frac{R^3}{r^3}, \tag{5}$$

where x_i is the position relative to the void's center along coordinate dimension i and $r = \sqrt{x_ix_i}$. Substituting Eq. (4) leads to manuscript Eq. (2):

$$\sigma_{ij} = \frac{1}{2}\sigma^H\left(\frac{R}{r}\right)^3\left(\delta_{ij} - \frac{3x_ix_j}{r^2}\right). \tag{6}$$

This stress state is maximized at the surface of the void, with principal stresses $\frac{1}{2}\sigma^H$, $\frac{1}{2}\sigma^H$, and $-\sigma^H$, giving a maximum shear stress of $\frac{3}{4}\sigma^H$.

The nature of the dislocation-void interaction due to Eq. (6) is dependent upon the character angle of the dislocation line and the height of the glide plane relative to the void equator [9]. Dislocations at the void equator experience no interaction force at all. Edge dislocations above and below the equator may be repelled or attracted, depending on the sign of the Burgers vector. With screw dislocations, one "half" of the dislocation line is attracted and the other half repelled, with the sign of the interaction swapping as the equator is crossed. Note that more than just the Schmid stress on the glide plane is important for this problem since other stress components strongly impact the cross-slip rate [10]. A final point is that Eq. (6) only describes the stress resulting from the applied hydrostatic stress. There is also a stress field due to the image interaction between the dislocation and the void. This image interaction is always attractive, and is not important here because it does not provide a driving force for void growth.

Void growth rates

We have calculated void growth rates under a constant applied hydrostatic stress. We find that when no dislocations are initially introduced and the stress is low enough that no dislocations nucleate at the void, the void does not grow. When dislocations are introduced, we find that the void does generally grow, with the rate of growth increasing as the dislocation density and hydrostatic stress increase. However, we find that for a fixed stress and dislocation density, the growth rate is tremendously sensitive to the configuration of the dislocation lines. This is not surprising, since adsorption-mediated growth depends on glide and cross-slip of dislocations near the void. In the manuscript, we presented the median growth rate among 20 different dislocation configurations for each stress and number of loops n. Here we present all of the MD results to demonstrate the significant scatter.

Fig. 3 presents the void growth rate as a function of hydrostatic stress for $n =$ (a) 18, (b) 36, and (c) 54 prismatic loops, and (d) 12 shear loops. We also provide semilog-y plots as insets for (b) and (c), since the spread in the data is so significant. The void growth rate for a given stress and number of dislocation loops varies by many orders of magnitude across the 20 runs. This broad variation in the $n = 36$ and 54 prismatic loop data sets leads to mean growth rates that do not vary in a consistent way with hydrostatic stress σ^H; a single large outlier growth rate pulls the mean away from the majority of the data. For this reason we have focused on the median value with these data sets, which is much less susceptible to outliers. The sensitivity to the details of the dislocation structure could be an important feature of adsorption-mediated growth. It may mean that certain types of dislocation cell walls/boundaries will be more conducive to void growth than others. It also implies that adsorption-mediated growth is a stochastic process, and so should be thought about in probabilistic terms.

References

[1] Plimpton S. Fast parallel algorithms for short-range molecular dynamics. J Comp Phys. 1995;117:1–19.

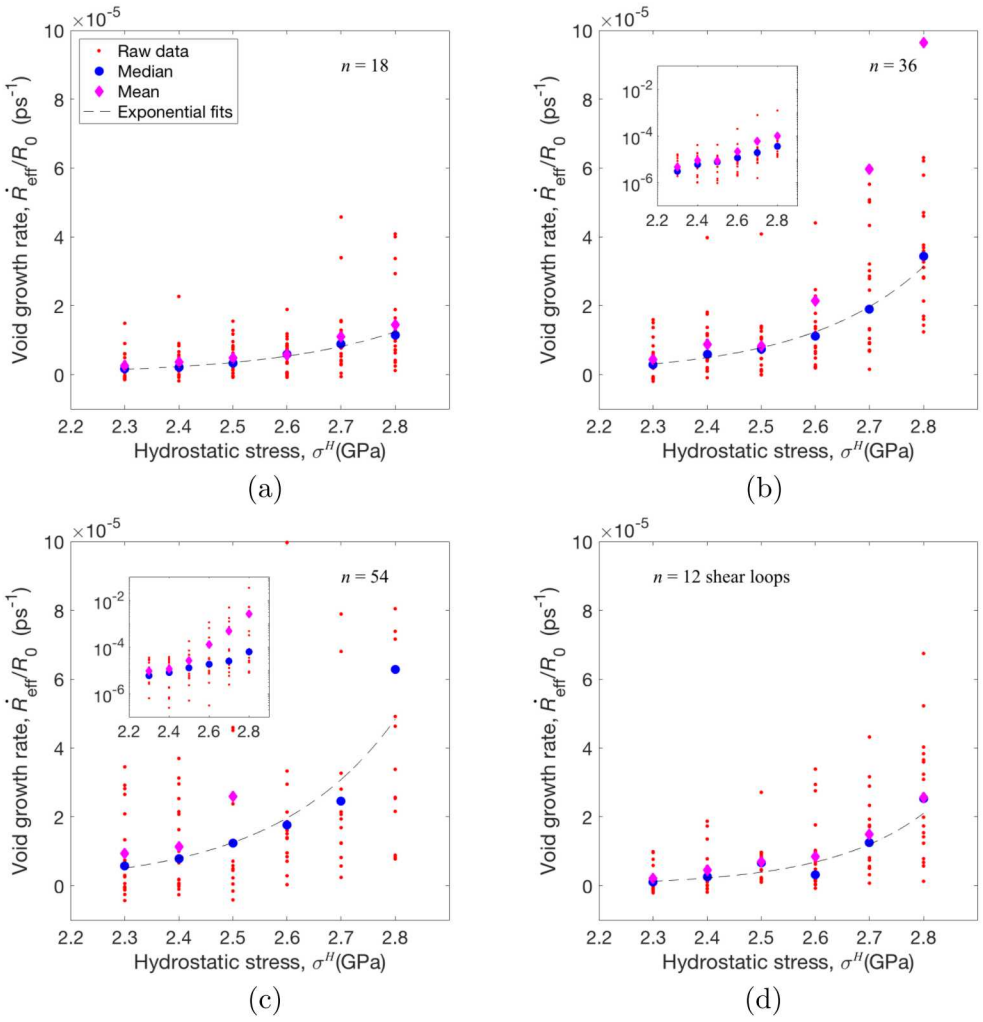

Figure 3. Void growth rates under a constant applied hydrostatic stress σ^H when $R_0 = 5$ nm, box edge length $L = 32.5$ nm and $n =$ (a) 18, (b) 36, and (c) 54 prismatic dislocation loops, and (d) 12 shear loops. The growth rate for each of the 20 runs at each condition is shown as dots, with the mean and median for each dataset also shown. Dashed lines are the same exponential fits shown in the manuscript. The insets in (b) and (c) show the full range of data in cases where some data points were out-of-range in the main graphs.

[2] Bulatov VV, Cai W. Computer simulations of dislocations. Oxford, UK: Oxford University Press; 2006.
[3] Barnett DM. The displacement field of a triangular dislocation loop. Phil Mag A. 1985; 51:383–387.
[4] Barnett DM, Balluffi RW. The displacement field of a triangular dislocation loop-a correction with commentary. Phil Mag Lett. 2007;87:943–944.
[5] Stukowski A. Visulatization and analysis of atomistic simulation data with Ovito: The Open Visulation Tool. Modelling Simul Mater Sci Eng. 2010;18:015012.
[6] Eshelby JD. Elastic inclusions and inhomogeneities. In: Sneddon IN, Hill R, editors. Progress in solid mechanics. Chapter 3. Amsterdam: North-Holland Publishing Company; 1961. p. 87–140.
[7] Mura T. Micromechanics of defects in solids. Norwell, MA: Kluwer Academic Publishers; 1987.
[8] Cai W, Sills RB, Barnett DM, et al. Modeling a distribution of point defects as misfitting inclusions in stressed solids. J Mech Phys Sol. 2014;66:154–171.
[9] Duesbery MS, Sadananda K. Interaction of dislocations with coherent inclusions. I. Perfect edge and screw dislocations. Phil Mag A. 1991;63(3):535–558.
[10] Kang K, Yin J, Cai W. Stress dependence of cross slip energy barrier for face-centered cubic nickel. J Mech Phys Solids. 2014;62:181–193.